ISPRS Journal of Photogrammetry and Remote Sensing 142 (2018) 137–150

Contents lists available at ScienceDirect

ISPRS Journal of Photogrammetry and Remote Sensing

journal homepage: www.elsevier.com/locate/isprsjprs

An empirical comparison of interpolation methods for MODIS 8-day land surface temperature composites across the conterminous Unites States

Timothy Pede, Giorgos Mountrakis*

SUNY College of Environmental Science and Forestry, Department of Environmental Resources Engineering, 419 Baker Lab, 1 Forestry Drive, Syracuse, NY 13210, United States

ARTICLE INFO

Keywords:
Land surface temperature
MODIS
8-day
Interpolation
Method assessment
Cloud

ABSTRACT

Eight-day composite land surface temperature (LST) images from the Moderate Resolution Imaging Specroradiometer (MODIS) sensor are extensively utilized due to their limited number of invalid pixels and smaller file size, in comparison to daily products. Remaining invalid values (the majority caused by cloud coverage), however, still pose a challenge to researchers requiring continuous datasets. Although a number of interpolation methods have been employed, validation has been limited to provide comprehensive guidance. The goal of this analysis was to compare the performance of all methods previously used for 8-day MODIS LST images under a range of cloud cover conditions and in different seasons. These included two temporal interpolation methods: Linear Temporal and Harmonic Analysis of Time Series (HANTS); two spatial methods: Spline and Adaptive Window; and two spatiotemporal methods: Gradient and Weiss. The impact of topographic, land cover, and climatic factors on interpolation performance was also assessed. Methods were implemented on high quality test images with simulated cloud cover sampled from 101 by 101 pixel sites (1-km pixels) across the conterminous United States.

These results provide strong evidence that spatial and spatiotemporal methods have a greater predictive capability than temporal methods, regardless of the time of day or season. This is true even under extremely high cloud cover (> 80%). The Spline method performed best at low cloud cover (< 30%) with median absolute errors (MAEs) ranging from 0.2 °C to 0.6 °C. The Weiss method generally performed best at greater cloud cover, with MAEs ranging from 0.3 °C to 1.2 °C. The regression analysis revealed spatial methods tend to perform worse in areas with steeper topographic slopes, temporal methods perform better in warmer climates, and spatiotemporal methods are influenced by both of these factors, to a lesser extent. Assessed covariates, however, explained a low portion of the overall variation in MAEs and did not appear to cause deviations from major interpolation trends at sites with extreme values. While it would be most effective to use the Weiss method for images with medium to high cloud cover, Spline could be applied under all circumstances for simplicity, considering that (i) images with < 30% cloud cover represent the vast majority of 8-day LST images requiring interpolation, and (ii) Spline functions are readily available and easy to implement through several software packages. Applying a similar framework to interpolation methods for daily LST products would build on these findings and provide additional information to future researchers.

1. Introduction

Land surface temperature (LST) is the radiative skin temperature of the land surface, measured through emitted thermal infrared radiation in the diction of a given remote sensor. LST has been widely utilized across various scientific disciplines for a variety of purposes, including climatology, hydrology, metrology, land cover/land use change analysis, urban heat island monitoring, and ecosystem health assessment (Ren et al., 2011; Huang et al., 2013; Xu et al., 2013; Fan et al., 2014; Metz et al., 2014; Van Nguyen et al., 2015; Ma et al., 2017) and is a key parameter in the physics of land surface processes on regional and global scales (Liang, 2001; Yu et al., 2014).

Traditionally, LST has been recorded by radiometers at weather stations, resulting in in-situ point data. Over the past several decades, however, global LST datasets have become available via satellite remote sensing. These earth observation missions include the Moderate Resolution Imaging Spectrometer (MODIS), the Advanced Very High Resolution Radiometer (AVHRR), and Advanced Along Track Scanning

* Corresponding author.
E-mail addresses: tjpede@syr.edu (T. Pede), gmountrakis@esf.edu (G. Mountrakis).

https://doi.org/10.1016/j.isprsjprs.2018.06.003
Received 8 January 2018; Received in revised form 18 April 2018; Accepted 6 June 2018
Available online 12 June 2018

Radiometer (AATSR) (Alfieri et al., 2013). If a researcher is interested in a large study area, satellite-derived LST is superior to readings from meteorological stations, especially in remote areas (Zeng et al., 2015). Although geostatistical methods are available for interpolation of ground observations, these can produce results with significant error due to invalid assumptions with regards to spatial averaging and the exclusion of topographic factors (Xu et al., 2013; Alfieri et al., 2013; Zhang et al., 2013; Zeng et al., 2015).

Due to its superior spatial and temporal resolution, MODIS has become the dominant satellite-based sensor for LST data (Ren et al., 2008; Zeng et al., 2016). The constellation consists of two identical sensors; one onboard the Terra satellite and another onboard the Aqua satellite. MODIS sensors estimate LST from thermal infrared bands using a split window algorithm (Li et al., 2012; Xu et al., 2013; Alfieri et al., 2013; Zeng et al., 2015). The Terra and Aqua combined sensors record the LST at each location up to 4 times a day at an approximately 1-km resolution (0.93-km); 1–2 times for the daytime temperature and 1–2 times for the nighttime temperature (Wan, 2008).

Daily MODIS LST images frequently contain invalid pixels as a result of cloud contamination (Yu et al., 2014; Metz et al., 2014). For cloudy regions, in particular, it is virtually impossible to accurately reconstruct a continuous time-series dataset (Van Nguyen et al., 2015). To overcome this issue, 8-day LST composites are available, which are derived from averaging all clear sky observations for a given pixel over an 8-day period. The high portion of missing pixels in daily LST images often makes it impractical for mapping purposes. Therefore, 8-day images are in many cases simpler to utilize and preferred (Hengl et al., 2012; Linghong et al., 2012). The use of 8-day images is also advantageous since it reduces storage space requirements and computation time. However, even these images can contain a large portion of invalid pixels. As there are numerous applications that require spatially and temporally continuous LST datasets (Qingbai and Yongzhi, 2004; Tomlinson et al., 2011; Linghong et al., 2012), several interpolation methods have been employed to fill gaps in composite images.

While a number of novel interpolation methods have been proposed for daily MODIS LST images (Neteler, 2010; Metz et al., 2014, Fan et al., 2014; Yu et al., 2015; Zeng et al., 2015; Shwetha and Kumar, 2016), our work focused on methods that have been used for 8-day composite images due to their wide applicability and easier utilization, as discussed above. Invalid values for 8-day LST composites have been interpolated over a variety of study areas, varying in both spatial and temporal extents (Refer to Table S.1 for more details). According to Metz et al. (2014), the interpolation of MODIS products can be categorized into three groups: spatial-based, temporal-based, and spatio-temporal-based. For temporal methods, invalid values are estimated on a pixel-by-pixel basis and do not consider values of geographically neighboring pixels. Spatial methods only consider the values of neighboring pixels and do not include values from different periods of time. Spatiotemporal methods consider pixels neighboring in both the temporal and spatial domain.

In terms of temporal interpolations, the Linear Temporal approach was utilized by Klingseisen (2010) and Zhang et al. (2015). For each missing pixel, the rate of change in LST between the closest proceeding and following 8-day periods with data are determined and used to construct a linear equation. Based on the temporal distance between the period in question and the LST of the closest proceeding period with data, the linear equation can be applied to fill the missing value. A more sophisticated temporal approach is Harmonic Analysis of Time Series (HANTS). This technique was originally developed for smoothing and gap-filling normalized difference vegetation index (NDVI) images, but has been used to interpolate invalid data in both daily (Maffei et al., 2012; Alfieri et al., 2013) and 8-day MODIS LST images (Xu and Shen, 2013; Xu et al., 2013; Van Nguyen et al., 2015). The algorithm uses a least squares curve fitting procedure based on harmonic components. For each harmonic, the amplitude and phase of the cosine function is determined during an iterative fitting procedure (Roerink et al., 2000).

In spatial interpolations, Linghong et al. (2012) proposed a novel method that relies on the assumption that LST is correlated with elevation. For each image, a moving window is used to interpolate invalid pixels based on the linear relationship with elevation. When a certain portion of cells within a window are valid, ordinary least squares (OLS) regression is performed, in which LST is modeled as a linear function of elevation. The LST is then interpolated based on the elevation of the center cell and the derived function. It is referred to as Adaptive Window, because this process continues after each pass until all pixels within an image are interpolated. This method was later applied by Zhang et al. (2013). Another spatial method for MODIS 8-day LST images is Spline interpolation. Three dimensional surface splines are used to interpolate a Z value (LST) for a given X and Y coordinate point. Both Hengl et al. (2012) and Kilibarda et al. (2014) used the *Close Gaps* function, available in System for Automated Geoscientific Analysis (SAGA) open source software (via the grid_tools module) for interpolation.

A simple Gradient spatiotemporal method for 8-day MODIS LST was first implemented by Hassan et al. (2007a, 2007b). This technique is based on temperature differences between the LST of pixels and average LST of images. For each 8-day image, the difference between the average LST (ie. average of all valid pixels) and each valid pixel is calculated. The average difference, or gradient, is then calculated on a pixel-by-pixel basis over a period of time. Missing values are filled by adding the average gradient of a pixel to the average LST of an 8-day image. Later studies used this approach to improve the quantification of growing degree days and surface wetness indices (Hassan et al. (2007a, 2007b) (2); Akther and Hassan, 2011; Rahman, 2011; Rahaman and Hassan, 2017)

Finally, a novel spatiotemporal approach was proposed by Weiss et al. (2014). Gaps are first filled by identifying proceeding and following calendar dates with a usable value for the gap pixel and searching outward for spatially neighboring pixels with valid values in both images. If the maximum search radius is reached without a pixel threshold being met, the search continues into calendar dates of proceeding and following years. Once the threshold is met, gap pixels are filled based on their LST from a given calendar date and the ratio of LST between images for neighboring pixels (inversely weighted by time-space distance). If all years are exhausted without the threshold being met, remaining pixels are filled using their average LST (computed across all years) and the ratio between the LST and multiyear average of valid spatially adjacent pixels within an iterative, multidirectional window. This technique, henceforth referred to as Weiss, has been extensively employed for epidemiology studies in various geographic regions (Pigott et al., 2015; Messina et al., 2015; Weiss et al., 2015; Mylne et al., 2015; Kraemer et al., 2015; Nsoesie et al., 2016; Golding et al., 2017; Longbottom et al., 2017).

The main limitation of studies that interpolated 8-day MODIS LST images is that assessment did not contrast an extensive number of methods and sites. There remains a need to compare the performance of methods across a variety conditions and using a common framework to assess interpolation accuracy across seasons, time of day, and site conditions. This study aimed to address this problem by empirically comparing six methods previously employed for interpolating invalid data in 8-day MODIS LST images (Linear Temporal, HANTS, Adaptive Window, Spline, Gradient, and Weiss). To the best of our knowledge, these constitute all methods that have been applied to 8-day MODIS LST. Our objectives were twofold: (1) determine which method is the best predictor of invalid 8-day LST pixels in daytime and nighttime images under a range of cloud cover and seasonality conditions and (2) assess how topographic, climatic, and land cover conditions impact their predictive power. The overarching goal was to provide an actionable guidance for scientists and practitioners with respect to the creation and usage of such datasets.

2. Methods

All six methods were applied to interpolate invalid data across eighty-five 101 by 101 pixel test sites (1-km pixels) sampled across the conterminous United States (CONUS); center pixels were used for assessment. Masks with varying levels of cloud cover were generated from observed imagery across sites and applied to test scenes with a high portion of valid data. Seasonality was incorporated by selecting masks and test scenes from all 4 seasons. To determine the impact of time of day, assessment was performed separately for daytime and nighttime LST images. Finally, a regression analysis was conducted to identify factors that significantly influence the predictive error of each method.

2.1. MODIS LST data and preprocessing

This study utilized 1-km 8-day composites from the MODIS sensor onboard the Terra satellite (MOD11A2 – version 6), which contain both daytime and nighttime LST images, as well as the corresponding Quality Assurance (QA) layers. Data from 2001 to 2016 was downloaded from the Daac2Disk tool for the CONUS, courtesy of the NASA EOSDIS Land Process Distributed Active Archive Center (LP DAAC, 2014). Tiles were mosaicked and raw LST values were converted to °C; the original sinusoidal coordinate system was kept and all additional base layers were reprojected to match.

Ocean pixels were identified using the QA layer and excluded from interpolation and cloud mask creation. Two base layers were used for the selection of test sites: the 250-m MODIS Water Mask (MOD44W), obtained from Carroll et al. (2009), and the Level III Ecoregion shapefile, obtained from US EPA (2013).

2.2. Study area and test sites selection

The CONUS was identified as an ideal study area due to its wide range of topographic and climatic conditions, in addition to the availability of auxiliary data. To ensure sufficient variation in environmental conditions, one test site was selected from each of the 85 Level III Ecoregions within the CONUS. These boundaries represent areas of similar ecosystems and are delineated by the US Environmental Protection Agency on the basis of geology, landforms, vegetation, climate, land use, wildlife, and hydrology (Omernik and Griffith, 2014).

To select high quality center test pixels, the MODIS Water Mask was used to exclude pixels containing any water. Center test pixels were selected by generating random points within the minimum bounding box of their corresponding Ecoregion until a point was found that fell within the inwardly buffered region, but outside of a 1-km LST pixel containing water. Study site grids were created by extracting the 50 pixels surrounding each side the selected test pixels. As there are 46 8-day periods in a given year and 16 years of MODIS data, there were 736 101 by 101 pixel images of daytime LST, daytime QA, nighttime LST, and nighttime QC for each study site. The footprint of all 85 sites is depicted in Fig. 1.

2.3. Artificial cloud creation and empirical assessment

Cloud masks were created based on the actual footprints, or patches, of cloud-contained pixels present in 8-day LST images from study sites. This replicated previously observed cloud coverage and artificially excluded LST data for interpolation. Twenty tests were performed for each site, season, and cloud cover category. It should be noted that in this case, cloud-contaminated and invalid are used interchangeably. While it is possible for invalid values to occur as a result of emissivity error, the vast majority for MODIS 8-day LST composites are derived from cloud obstruction (> 99%). Seasons were defined as meteorological seasons (*Winter* = January, February, December; *Spring* = March, April, May; *Summer* = June, July, August; *Fall* = September, October, November) and assigned to images based on the season of the first day of the 8-day period. Ten cloud cover categories in equal increments were utilized, ranging from (0–10%) to [90–100%). Thus, interpolation methods were assessed for daytime and nighttime images with 800 tests per site (20 tests × 10 categories × 4 season). For a given season, category, and time of day, there were 1700 tests across all sites (20 tests × 85 sites).

Twenty masks were generated for each cloud cover category and season using imagery from study sites. Selected images contained an invalid center pixel and corresponding portion of invalid cells. Since there were an insufficient number of images meeting these criteria to

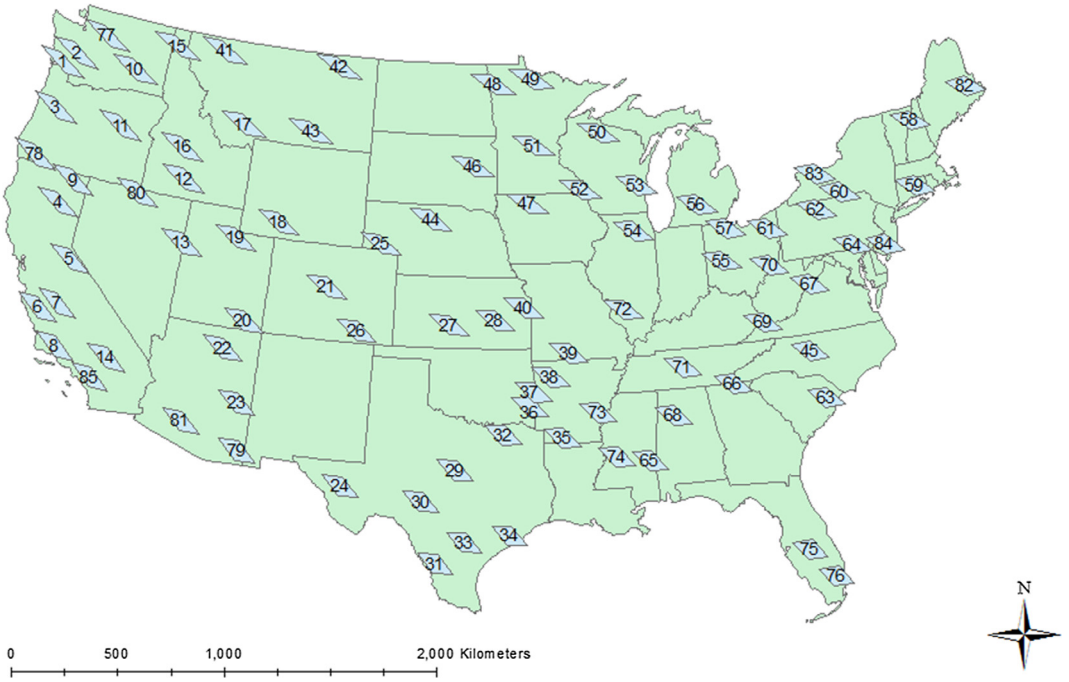

Fig. 1. Footprint of the 85 101 by 101 pixel (1-km pixels) utilized study sites and Ecoregion number. The shape of the footprints is attributed to the MODIS sinusoidal projection. Refer to US EPA (2013) for the name corresponding to each Ecoregion number.

utilize site-specific masks, a single set of masks was compiled from all sites. For each season and category, candidate masks were identified and sites with a potential mask were randomly selected. This avoided multiple masks coming from a single site. If there were less than 20 sites, this process was repeated for sites having multiple candidate masks until 20 were selected. This was done separately for daytime and nighttime LST to derive daytime and nighttime cloud masks. Sites containing ocean pixels were not used to derive cloud masks.

Test scenes (ie. validation images) for seasons were identified for sites where the center pixel was high quality (QA = 00) and the portion of invalid pixels was 0%. If there were at least 20 images from 2001 to 2016 that met this criteria, twenty were randomly selected. If there were less than 20, images that met the criteria were kept and additional images were found where the center pixel was high quality and the portion of invalid pixels was < 1%. This continued until 20 images were found, according to the criteria listed in Table S.2. Test scenes from the vast majority of sites were found where the center pixel was high quality. Through this process, sites were assigned 20 daytime and nighttime test scenes for all 4 seasons.

Once cloud masks and test scenes were selected, the validation process was performed. Invalid pixels were simulated by applying the 20 masks for each cloud cover category and season to each site's corresponding test scenes. Pixels in test scenes were set to invalid if the same pixel was invalid in the applied cloud mask (as depicted by Fig. 2). The 6 interpolation methods were then implemented to predict the LST of center test pixels. To reduce the influence of outliers, performance was assessed using the median absolute difference (i.e. error) between predicted and observed LSTs across all sites for each cloud cover category and season.

2.4. Assumptions and implementation of interpolation methods

Linear Temporal: Following the procedure described by Klingseisen (2010) and Zhang et al. (2015), the closest proceeding and following 8-day periods with valid data were identified and used to derive a linear equation to estimate the missing LST value of the test pixel. Since it is rare for a pixel to have an invalid LST value for 2 consecutive 8-day periods, most estimation was accomplished by a simple average of the two values immediately neighboring in time.

Harmonic Analysis of Time Series (HANTS): Five input parameters are required by the user for the HANTS algorithm: the number of frequencies (NOF), high/low suppression flag (SF), valid data range (VDR), fit error tolerance (FET), and degree of over-determinedness (DOD) (Roerink et al., 2000). A value of 'Low' was used for SF, since undetected clouds result in unusually low LST values (Alfieri et al., 2013; Van Nguyen et al., 2015). A range of −50 °C to 70 °C was set for VDR to omit unusual temperatures for the CONUS. Values of 6 °C and 7 °C were used for the FET and DOD, respectively (Xu and Shen, 2013; Xu et al., 2013; Van Nguyen et al., 2015). Although some authors recommend an initial assessment to find an optimal NOF value (Xu and Shen, 2013; Van Nguyen et al., 2015), this would have been unfeasible due to the high number of sites. We used 2 to reflect annual and semiannual cycle harmonics (Xu et al., 2013). The HANTS algorithm was applied to individual years since, as noted by Maffei et al. (2012), derived coefficients can vary significantly from year-to-year. Once a cloud mask was applied to a validation image, LST values of the center pixel were compiled into a time-series. The value from the fitted curve corresponding to the 8-day period of the test image was used as the predicted value. We utilized the HANTS Matlab function created by Abouali (2012).

Adaptive Window: The Adaptive Window method was applied using a sliding window size of 49 by 49 pixels and 10% threshold for the portion valid pixels needed for regression (as used by both Linghong et al., 2012; Zhang et al., 2013). A resampled and filled 1-km DEM from the NASA Shuttle Radar Topography Mission (SRTM) was employed (Jarvis et al., 2008). The layer was reprojected to the sinusoidal coordinate system (via nearest neighbor resampling) and snapped to the MODIS LST grid by taking an average of coincident points. The MODIS Water Mask was used to identify LST pixels that were majority water to omit from validation. Once a mask was applied, images were filtered based on the QA layer (QA = 00) and histogram to eliminate unusually high and low outliers. Some checks were necessary to avoid over-filtering. There were 7 sites where QA filtering was not performed, since they had very few high quality LST readings due to the geometry of the area. QA filtering was also not performed if there were no high quality pixels in a given image.

Spline: While previous authors have employed SAGA GIS for spline interpolation (Hengl et al., 2012; Kilibarda et al., 2014), this analysis utilized the *Griddata* function in Matlab. Surfaces were fit to test scenes and used to predict the value of the center test pixel. Biharmonic Spline was specified as the method ('v4'), since it is not based on triangulation and thus, the most sophisticated and mathematically rigorous option available.

Gradient: Similar to HANTS, the Gradient method was implemented on an annual basis, such that all 46 8-day images in the year of a given validation image were used to calculate the average LST offsets for pixels. The average offset was calculated for center pixels following the application of the cloud mask. Averages were calculated using an entire year of data, a slight deviation from Hassan et al. (2007a, 2007b), who only used 8-day images from the growing season (April 7th–October 31st).

Weiss: It was necessary to compile an image stack for each calendar date across all years from 2001 to 2016 (16 calendar dates for each 8-day period). Outlying LST values were initially identified and set to invalid on a pixel-by-pixel basis using their z-score (if z-score > 2.58). Mean pixel-by-pixel values were computed across all 16 years. As

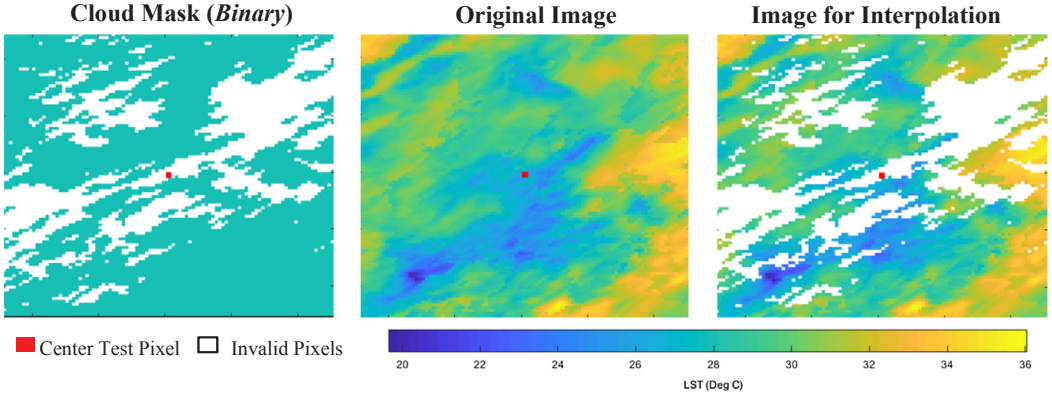

Fig. 2. Visual example of cloud cover simulation for selected test and center test pixel to interpolate (Daytime LST, Site 24, Winter, 28.4% cloud cover – 20–30% category).

implemented by Weiss et al. (2014), values of 40 and 80 were used as the minimum and maximum thresholds, respectively, along with a 3.6-km search radius (corresponding to roughly a 7 by 7 pixel window).

2.5. Assessment of topographic, land cover, and climatic factors

To identify potential factors that influence the performance of interpolation methods, a regression analysis was conducted between obtained errors and various topographic, land cover, and climatic variables. Based on images from selected study sites, the vast majority with cloud cover contained less than 30% (86.8% and 88.6% for daytime and nighttime images, respectively). For simplicity, median absolute errors (MAEs) for each site were computed from test results aggregated across all seasons and the first 3 cloud cover categories: (0,10%), [10,20%), and [20,30%). This resulted in sites having a single daytime/nighttime MAE for each of the 6 methods.

The source and spatial resolution of utilized covariates are summarized in Table S.3. The strong correlation between elevation and LST is well documented (Van De Kerchove et al., 2013; Stroppiana et al., 2014; Mathew et al., 2017; Khandelwal et al., 2017). Certain interpolation methods may perform better at lower or higher elevations. Likewise, methods may perform worse if there is significant change in elevation across a study area. The relationship between LST and land cover is also well documented, with vegetative cover generally having a lower LST on average than impervious cover (Tang et al., 2011; Guo et al., 2012; Wu et al., 2013; Qiao et al., 2013; Clinton and Gong, 2013). It is important to consider the effects of land cover on the discussed methods. To date, there has been no assessment of how interpolation methods perform in different climates. If a region experiences infrequent precipitation and limited cloud coverage, temporal methods may outperform spatial and spatiotemporal methods.

In terms of data processing, covariate layers were projected to the sinusoidal coordinate system (via nearest neighbor resampling), aggregated to a 1-km cell size, and snapped to MODIS pixels. Slope was computed from the SRTM DEM and matched to the MODIS grid as well. For continuous variables, aggregation was accomplished by taking an average of coincident points. For discrete land cover variables, NCLD classes were converted to binary layers via the scheme in Table S.3 and the percentage of each class was calculated for LST pixels. To summarize covariates as a single value for each site, a weighted (inverse distance) average was computed, giving pixels closer to the center a higher weight. This limited the influence of faraway values, since interpolation was only assessed on center pixels.

Once the covariates were determined, ordinary least-squares (OLS) regression was applied to develop a total of 12 models (a daytime and nighttime model for the 6 methods), such that each site was an observational unit, the aggregated MAE (in °C) was the dependent variable, and the covariates were the explanatory variables. To assess the relative influence of covariates, dependent and independent variables were standardized (subtracted mean and divided by standard deviation). Variation Inflation Factor (VIF) examination followed to reduce multicollinearity. OLS assumptions for uncorrelated residuals, homogenous variance, and normally distributed residuals were checked using the Durbin-Watson, White, and Kolmogorov-Smirnov tests, respectively.

3. Results and discussion

3.1. Performance of interpolation methods under varying cloud cover and seasons

Fig. 3 displays the median absolute error (MAE) for each method by cloud cover category and season when applied to daytime LST images. Depending on the method, season, and category, MAE values ranged from 0.27 °C to 3.66 °C. In general, the Spline spatial method had the lowest MAE for categories containing less than 30% cloud cover; at greater cover, the Weiss spatiotemporal method had the lowest MAE. Results were similar when interpolation methods were applied to

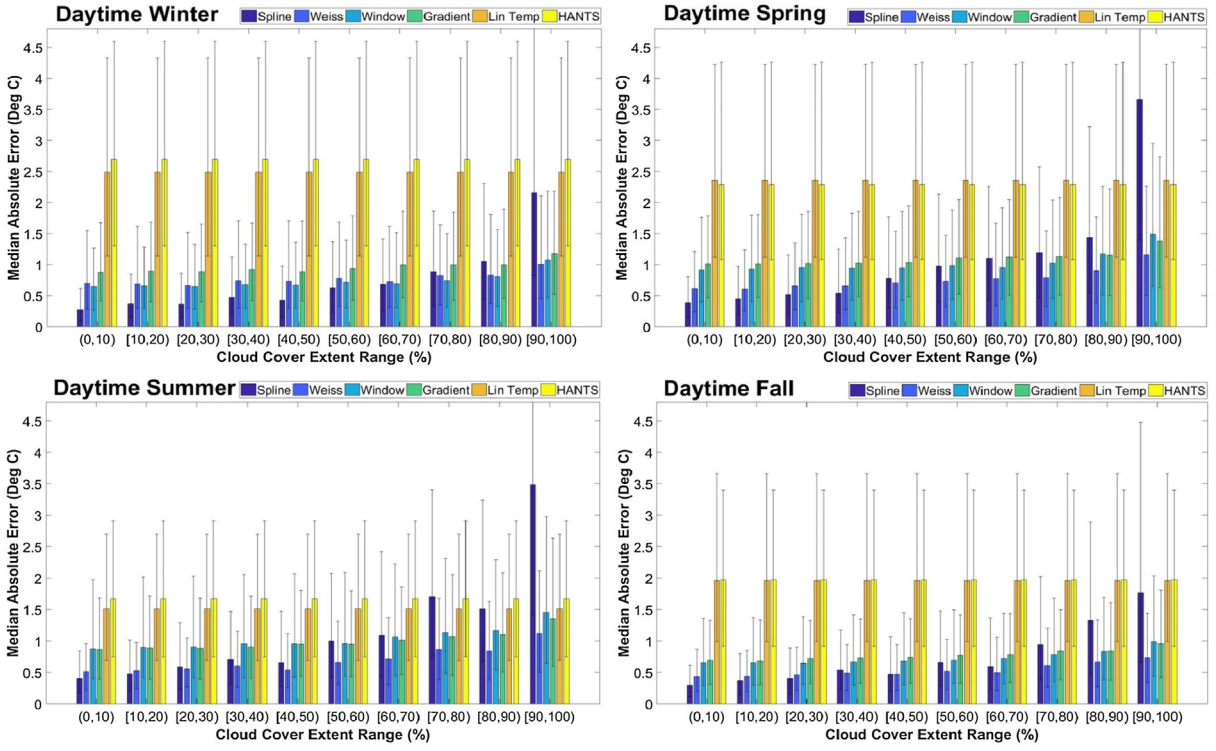

Fig. 3. MAEs and 75th/25th percentiles by cloud cover category and season for methods applied to daytime LST. Bins contain 1700 samples (20 tests at 85 sites); a small portion of tests (< 0.3%), especially for [90–100%), could not be completed for some spatial methods. Note: 75th percentiles of 5.6 °C, 10.6 °C and 8.5 °C not shown for last category for Spline method. Created using function by Callaghan (2014).

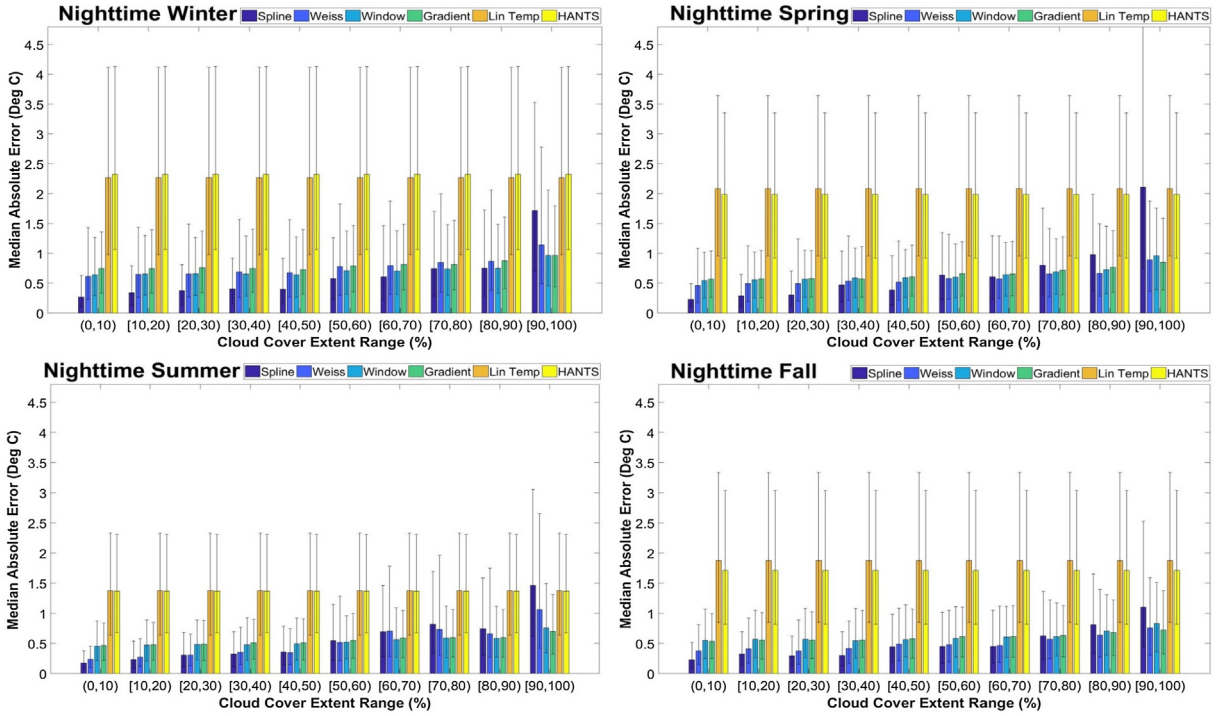

Fig. 4. MAEs and 75th/25th percentile by percent cloud cover category and season for methods applied to nighttime LST. Most bins contain 1700 samples (20 tests at 85 sites); a small portion of tests (< 0.2%), especially for [90–100%), could not be completed for some spatial methods. Note: 75th percentile of 10.9 not shown for last category of spring Spline. Created using function by Callaghan (2014).

nighttime images, only Spline had the lowest MAE up to the 40–50% cloud cover category and Weiss, Adaptive Window, or Gradient had the lowest MAE at greater cover, with relatively small separation in values (Fig. 4).

The MAE values for Spline, Adaptive Window, and Gradient were similar across seasons. Weiss exhibited minor improvement with fall and summer images, in the 0.01 °C to 0.33 °C range, causing it to have a lower MAE than Spline for the [20–30%) daytime summer category (by 0.03 °C). The MAE for the temporal methods, however, was quite lower for summer and fall LST images compared to winter and spring images; in some cases, by almost 1 °C. This is most likely due to less frequent cloud cover during these months, resulting in a greater number of values neighboring in time. While temporal MAEs for these seasons were lower, they were still greater than the MAEs of other methods, even for categories with high cloud cover. Although there were some exceptions, the best predictor for a given cloud cover category remained constant across seasons.

These findings provide strong evidence that spatial and spatiotemporal methods are capable of predicting cloud contaminated MODIS 8-day LST images with considerably less error than temporal methods. The higher predictive ability of the spatial domain may be attributed to the strong spatial dependency of LST. For variables that exhibit spatial dependency, or spatial autocorrelation, locations that are closer in space have similar values; locations further apart have less similar values (Cai and Wang, 2006). The spatial structure of LST is, in part, caused by its strong correlation with topographic and environmental factors (Neteler, 2010; Linghong et al., 2012; Zhang et al., 2013; Metz et al., 2014; Fan et al., 2014; Yu et al., 2014). These covariates also exhibit spatial autocorrelation. By only considering values neighing in time, temporal methods omit important information related to this spatial structure of LST. Furthermore, the 8-day (instead of daily) temporal interval further reduces temporal correlations.

Prediction improved for all methods with nighttime images, but Spline, Adaptive Window, and Gradient saw the greatest improvement. As a result, Spline remained the best predictor for categories containing < 50% cloud cover, with the exception of summer images (as opposed to 30% for daytime images). Adaptive Window and Gradient outperformed Weiss for some medium to high cloud cover categories as well, though the difference in MAEs was relatively small (typically < 0.1 °C). This improved performance may result from the more prominent spatial structure of LST at night. As authors have noted a stronger correlation between nighttime LST and elevation than daytime LST and elevation (Van De Kerchove et al., 2013; Stroppiana et al., 2014), topography and other environmental factors likely have a greater influence on nighttime LST. Although Gradient is classified as spatiotemporal, interpolated values are more reflective of the spatial domain, since the technique employs average offsets computed over time.

We expected to find a cloud cover range beyond which the temporal methods would outperform other techniques. However, with the exception of Spline for the last category [90–100%), temporal methods always produced a higher MAE. To investigate further we compared the spatial and temporal domains. Following the cloud mask application (with data pooled across seasons) it was revealed that the spatial average of remaining pixels is consistency closer to the value of the center test cell than the temporal average of the closest proceeding and following center pixels (Fig. 5). In fact, two-sample *t*-tests showed that the difference between the temporal and spatial domain mean was significant for all 10 categories with both daytime and nighttime images (for $\alpha < 0.01$). Thus, LST values of the same image within a 50-km radius of an invalid cell are more predictive than LST values neighboring in time, even under high cloud cover.

One explanation for the poor performance of temporal methods is that a time step of 8 days is too long to solely consider values neighboring in the temporal domain. Depending on how many daily readings are used to derive clear-sky composites, the two immediately neighboring 8-day pixels could be produced from daily images captured up to 24 days apart. This has important ramifications, considering HANTS is commonly used to interpolate missing values in both 8-day and daily MODIS LST images. Although it is widely accepted that HANTS can be

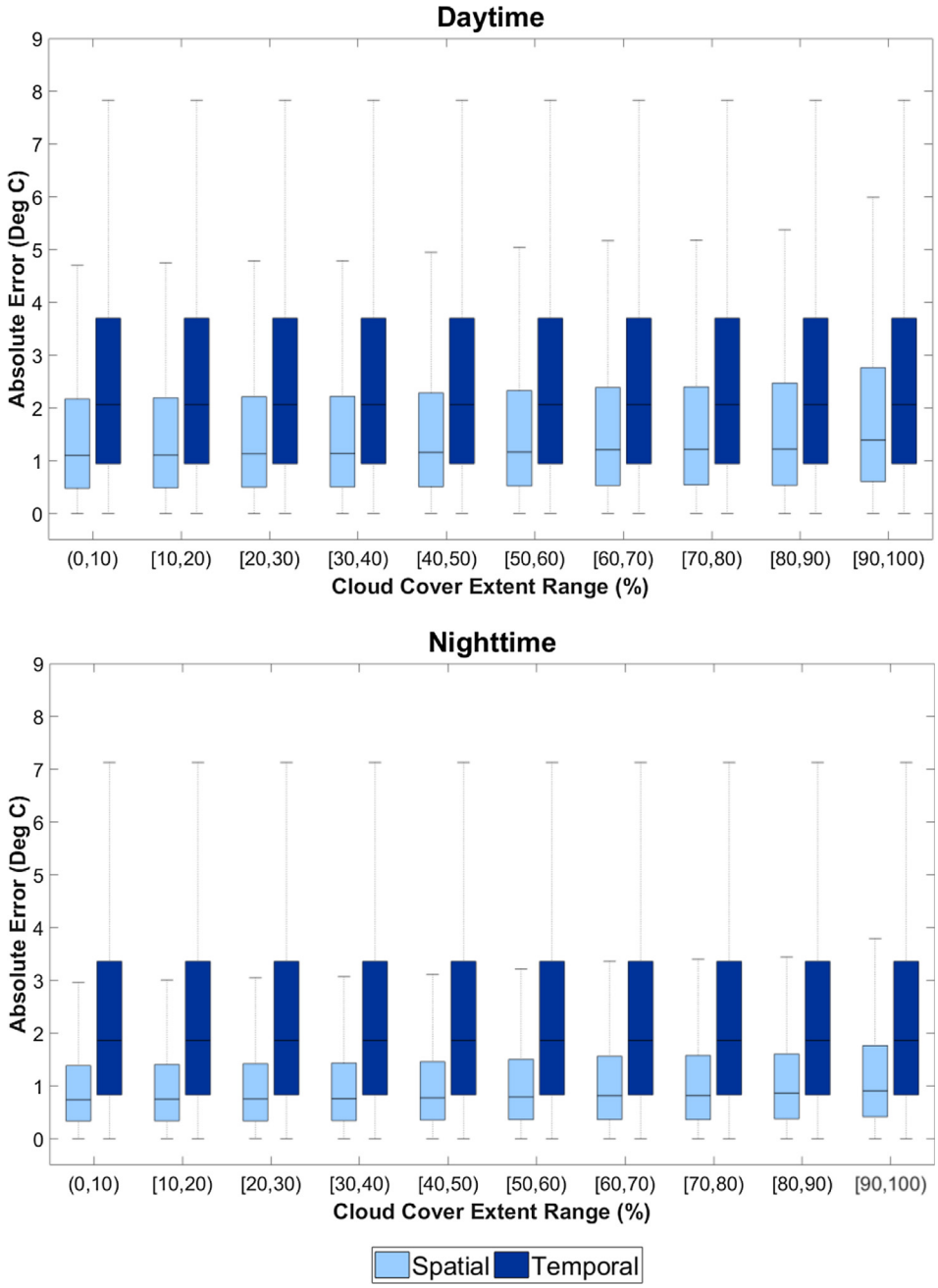

Fig. 5. Boxplots of absolute error between center test pixels and spatial and temporal domain averages by cloud cover category, pooled across sites and seasons. Outliers are not displayed. Created using function by Bikfalvi (2012).

employed for interpolating and smoothing remotely-sensed NDVI time series datasets (Poggio et al., 2012; Michishita et al., 2014; Zhou et al., 2016; Liu et al., 2017), we caution its use for interpolating 8-day LST images. The nature of composite LST time series data is too stochastic to be represented by a trigonometric function. In fact, HANTS performed no better than the simple Linear Temporal methods.

Our finding that spatiotemporal methods did not produce considerably lower MAEs deviates from trends amongst daily interpolation methods to incorporate both the spatial and temporal domain (Neteler, 2010; Metz et al., 2014, Yu et al., 2015; Shwetha et al., 2016). As discussed, a time step of 8-days is too long for LST values neighboring in time to provide useful information for prediction. Since composites represent clear-sky readings averaged over 8-days, spatial methods to some extent already consider the temporal domain. Furthermore, unlike gaps in daily LST images, which resemble the shape of clouds, composite gaps tend to be smaller and more scattered, as they only occur when there are no readings over the 8-day period. Under low to medium cloud cover, this decreases the distance between valid and invalid pixels; under high cloud cover, this results in a wider spatial distribution of valid pixels. Using combined spatial and temporal information does, however, provide slight improvement in most cases under medium to high cloud cover ($> 30\%$).

Considering previous authors' emphasis on incorporating topographic and environmental factors to interpolate MODIS LST images, especially elevation, it was surprising that Adaptive Window did not produce lower MAEs than Spline. While it performed reasonably well and better than the temporal methods, it generally produced higher MAEs at low to medium cloud cover ($< 60\%$). A more robust regression approach may be needed to model the relationship between elevation and LST, such as generalized least squares or autoregressive integrated

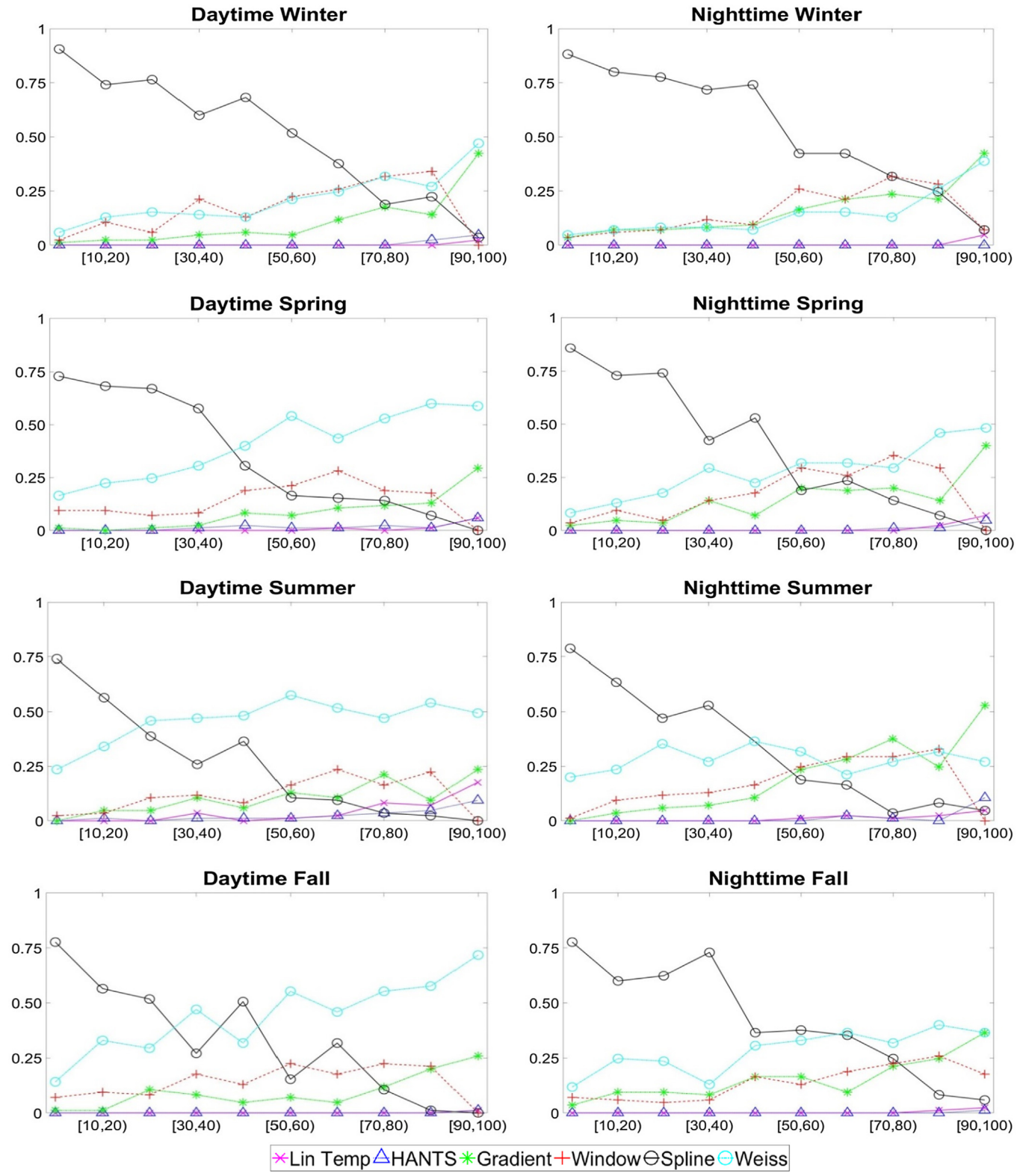

Fig. 6. Portion of sites for which each method performed best (Y-axis) for cloud cover categories (X-axis) by time of day and season.

moving average (ARIMA). It is also possible that for 8-day composite images, it is not necessary to consider topographic covariates.

Rather than computing the MAE from observations compiled across all sites, an alternative form of assessment is counting the number of sites for which a particular method had the lowest MAE. For the first cloud cover category (< 10%), Spline performed best for the vast majority of sites (> 70%) and, with the exception of daytime summer images, maintained the greatest portion at least until 30% (up to 70%) cloud cover (Fig. 6). For daytime images, Weiss generally performed best for the greatest portion of sites at medium to high cloud cover. However, there was little separation between Weiss, Gradient, and Adaptive Window for these categories with nighttime images. This is likely due to the stronger spatial dependency of nighttime LST and improved performance of spatial methods, as discussed previously.

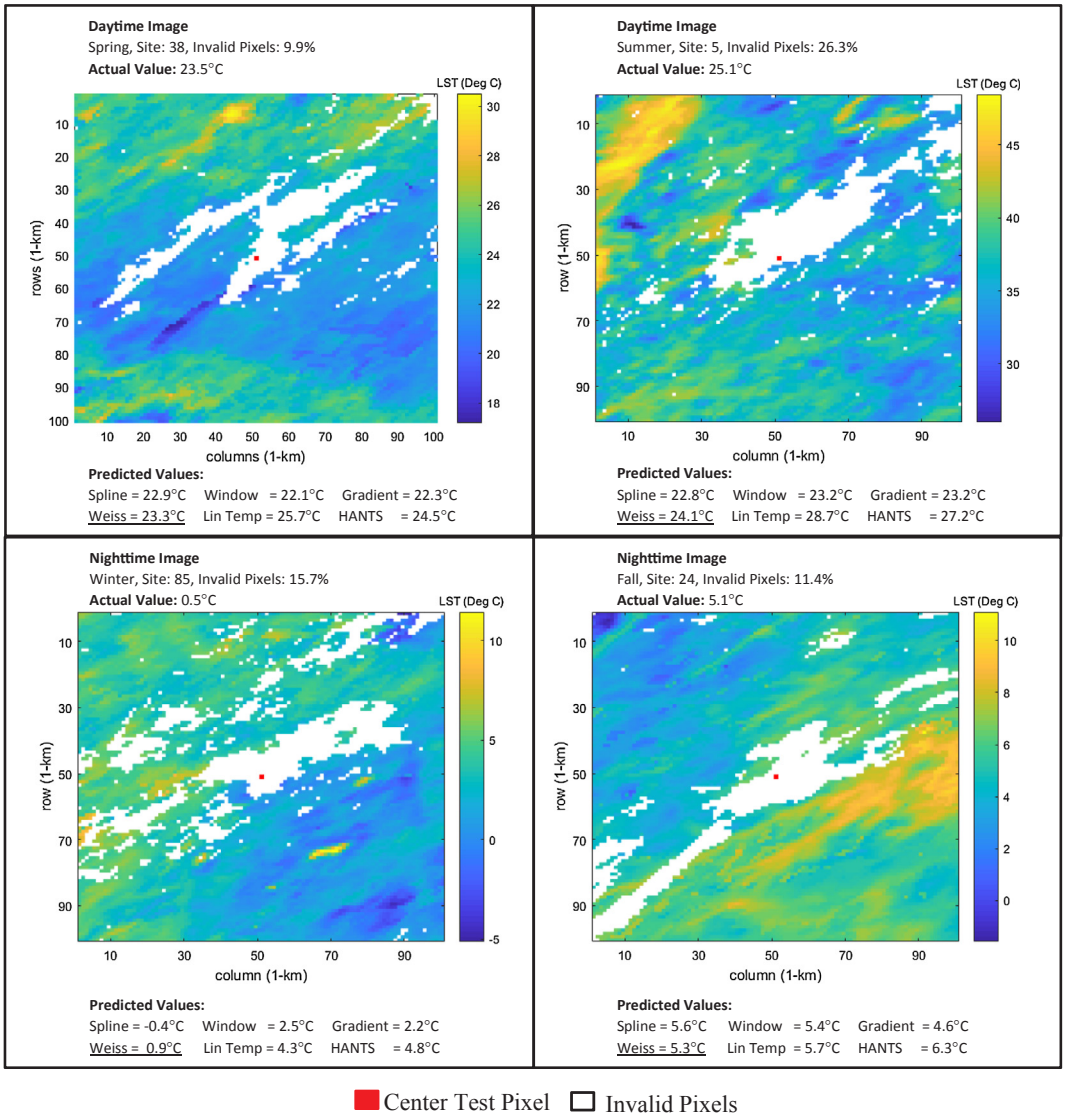

Fig. 7. Examples of interpolation results for images following cloud mask application with a concentration of invalid pixels around the center test cell. Refer to Fig. 1 for location of sites.

While there is no clear indication of the most appropriate method at medium to high cloud cover for nighttime images, this assessment clearly indicates that at low cloud cover (< 30%), Spline is the best interpolation method across the CONUS, regardless of the season or time of day. This is an important finding, considering that the majority of observed cloud coverage scenarios fell in this range.

As cloud cover was classified by the percent of obstructed pixels across the entire study area, this did not consider gap sizes surrounding center tests pixels. To further investigate the effects of gap size, we quantified the number of sites for which each method produced the lowest absolute error for low cloud cover masks (< 30%) and compared this to the portion of invalid cells within a 15-by-15 pixel buffer of the center pixels. Spline produced the lowest error at the most sites for 75.0% and 75.8% of daytime and nighttime low cloud cover masks, respectively; Weiss produced the lowest error at the most sites for 19.6% and 14.2%, respectively.

Low cloud cover masks for which Weiss performed better typically had a concentration of invalid pixels around the center (Fig. 7). In fact, the median portion of invalid pixels within the buffer when Spline performed best was 22.0% for daytime masks and 24.0% for nighttime masks, verses 38.1% and 35.4% for Weiss. The use of Weiss may be appropriate if there are extensive gaps surrounding interpolation pixels, most likely due to the iterative, multidirectional averaging windows. However, these instances are infrequent under low cloud cover, since invalid pixels tend to be scattered with 8-day composites. In addition, error improvements over Spline under these circumstances were small, with medians of 0.36 °C for daytime images and 0.23 °C for nighttime images.

A common concern among authors is that interpolation methods may only be applicable to clear-sky conditions, yet they are utilized to interpolate the LST of pixels obstructed by clouds (Hassan et al., 2007a, 2007b; Crosson et al., 2012; Zhang et al., 2013; Xu and Shen, 2013; Metz et al., 2014; Yu et al., 2014; Zeng et al., 2015). In other words, they assume that the LST of pixels not covered by clouds can be used to predict the LST of pixels that are covered by clouds. Invalid pixels may actually have a lower temperature. In order to assess how these methods predict LST under cloud cover, it would be necessary to compare predicted values to ground-based meteorological stations that record LST. There are two limitations to this approach; the first is the inability to discern error caused by interpolation from error inherent in remotely sensed LST. The process of estimating LST with a space born-sensor is subject to geometric and atmospheric distortion not encountered with ground-based LST measurements (Akhoondzadeh and Saradjian, 2008). The second is a lack of meteorological stations that

Table 1
Summary of covariates utilized for the error analysis.

Variable	Definition	Program	Spatial resolution	Units
Elev	Average elevation	SRTM	1-km	m
Slope	Average slope	SRTM	1-km	%
PerAg	Average percent agriculture (class = 81, 82)	NLCD	30-m	%
PerDev	Average percent developed (class = 21, 22, 23, 24)	NLCD	30-m	%
PerFor	Average percent forest (class = 41, 42, 43)	NLCD	30-m	%
PerWet	Average percent wetland (class = 90, 95)	NLCD	30-m	%
PerWat	Average percent water (class = 11)	NLCD	30-m	%
Temp	Average 30-year normal mean annual air temperature	PRISM	800-m	°F
MinTemp	Average 30-year normal minimum annual air temperature	PRISM	800-m	°F
MaxTemp	Average 30-year normal maximum annual air temperature	PRISM	800-m	°F
Percip	Average 30-year normal annual precipitation	PRISM	800-m	inch

Note: SRTM = Shuttle Radar Topography Mission (from Jarvis and Reuter (2008)), NLCD = National Land Cover Database (2011) (from USGS (2017), refer for class definitions), PRISM = Parameter-elevation Regressions on Independent Slopes Model (obtained from PRISM Climate Group (2004)).

record LST. For the CONUS, there is only the Climate Reference Network (CRN), which is comprised of just 93 stations with consistent year-to-year data, does not contain readings prior to 2013, and is limited to areas dominated by forest or agriculture (US DOC, 2002).

3.2. Error distribution across topographic, land cover, and climatic factors

Multiple linear regression was performed to link topographic, climatic, and land cover factors with obtained errors of the assessed methods; results are displayed in Table 2 (for variable abbreviations see Table 1). Scatter plots between independent and dependent variables appeared to be linear or have a low degree of association. It was necessary to eliminate MinTemp and MaxTemp, since they had a Variance Inflation Factor of more than 10, due to their high correlation with Temp. Durbin-Watson (DW) tests revealed that autocorrelation was not a concern in any model because DW values were within the commonly accepted range of 1.5–2.5 (Alkorta et al., 2000; Zakerian and Subramaniam, 2009; Bakon and Hassan, 2013; Al-Matari et al., 2014; Venkathaialam and Abdulwahab, 2017). Based on White tests, heteroscedasticity was not significant in any of model (for $\alpha = 0.1$).

Most models had non-normal residuals, likely due to several positively skewed independent and dependent variables. To rectify this, any variable that significantly deviated from the normal distribution (based on the Kolmogorov-Smirnov test for $\alpha = 0.05$) was transformed via the natural log function. This included the dependent variables of daytime/nighttime Spline, Gradient, and Weiss MAE and independent variables of Elev, Slope, PerAg, PerDev, PerFor, PerWet, and PerWater. A negative reciprocal transformation was needed for daytime/nighttime Window MAE since resulting model residuals were still positively skewed when these dependent variables were initially log transformed. The negative ensured that positive and negative coefficients corresponded to direct and inverse relationships, respectively. Following variable transformation, the residuals for all models did not significantly deviate from a normal distribution (for $\alpha = 0.05$).

All models had an overall significance for $\alpha = 0.01$, with the exception of the nighttime Window model, which was significant for $\alpha = 0.05$, meaning β was significantly different than 0 for at least one variable. The daytime model explained a higher portion of variation in MAEs than the nighttime model for HANTS, Window, and Gradient. This suggests that the assessed factors have a greater influence on the predictive capability of these methods during the day. The opposite was true for other methods.

Significant variables differed by method and time of day. However, some major trends are apparent. Based on the standardized coefficient, Slope had the most influence on both daytime and nighttime MAEs for Spline and Adaptive Window. The positive value indicates that spatial methods perform better in flatter study areas. As stated previously, there is a strong correlation between LST and elevation. If there is more variation in elevation, there will also be more variation in LST. For Spline, this may cause fit surfaces to be less predictive, since there are larger discrepancies between the LST of neighboring pixels. It is also possible that for the Adaptive Window method, this increased variation causes the relationship between LST and elevation to become nonlinear and not as well captured with a linear model.

Table 2
Significant coefficients from OLS regression. For full models, refer to Tables S.3. Variable significance: $^{\wedge}\alpha = [0.05,0.1]$, $^{*}\alpha = [0.01,0.05)$, $^{**}\alpha \leq 0.01$.

Daytime Models

Linear Temporal Adj R^2: 0.411		**HANTS** Adj R^2: 0.4622		**Spline** Adj R^2: 0.297		**Window** Adj R^2: 0.251		**Gradient** Adj R^2: 0.282		**Weiss** Adj R^2: 0.474	
Term	*Coef*	*Term*	*Coef*	*Term*	*Coef*	*Term*	*Coef*	*Term*	*Coef*	*Term*	*Coef*
Constant	0.000^{**}	Constant	0.000^{**}	Slope	0.762^{**}	Slope	0.710^{**}	Slope	0.447^{*}	PerAg	$0.245^{\wedge}$
Temp	-0.733^{**}	PerWat	$-0.248^{\wedge}$	PerFor	-0.384^{**}	PerWat	-0.326^{*}	PerFor	-0.312^{*}	PerDev	$-0.278^{\wedge}$
		Temp	-0.705^{**}			PerWet	0.436^{**}	PerWet	0.385^{*}	Temp	-0.469^{**}

Nighttime Model

Linear Temporal Adj R^2: 0.505		**HANTS** Adj R^2: 0.401		**Spline** Adj R^2: 0.457		**Window** Adj R^2: 0.120		**Gradient** Adj R^2: 0.216		**Weiss** Adj R^2: 0.502	
Term	*Coef*	*Term*	*Coef*	*Term*	*Coef*	*Term*	*Coef*	*Term*	*Coef*	*Term*	*Coef*
Constant	0.000^{**}	Constant	0.000^{**}	Slope	0.802^{**}	Slope	0.564^{**}	Temp	-0.425^{*}	Slope	0.421^{**}
Slope	-0.383^{*}	Slope	-0.550^{**}	PerFor	$-0.214^{\wedge}$					Temp	-0.618^{**}
PerAg	0.435^{**}	PerAg	$0.253^{\wedge}$	Temp	-0.369^{**}						
Temp	-0.729^{**}	Percip	0.301^{*}								
		Temp	-0.575^{**}								

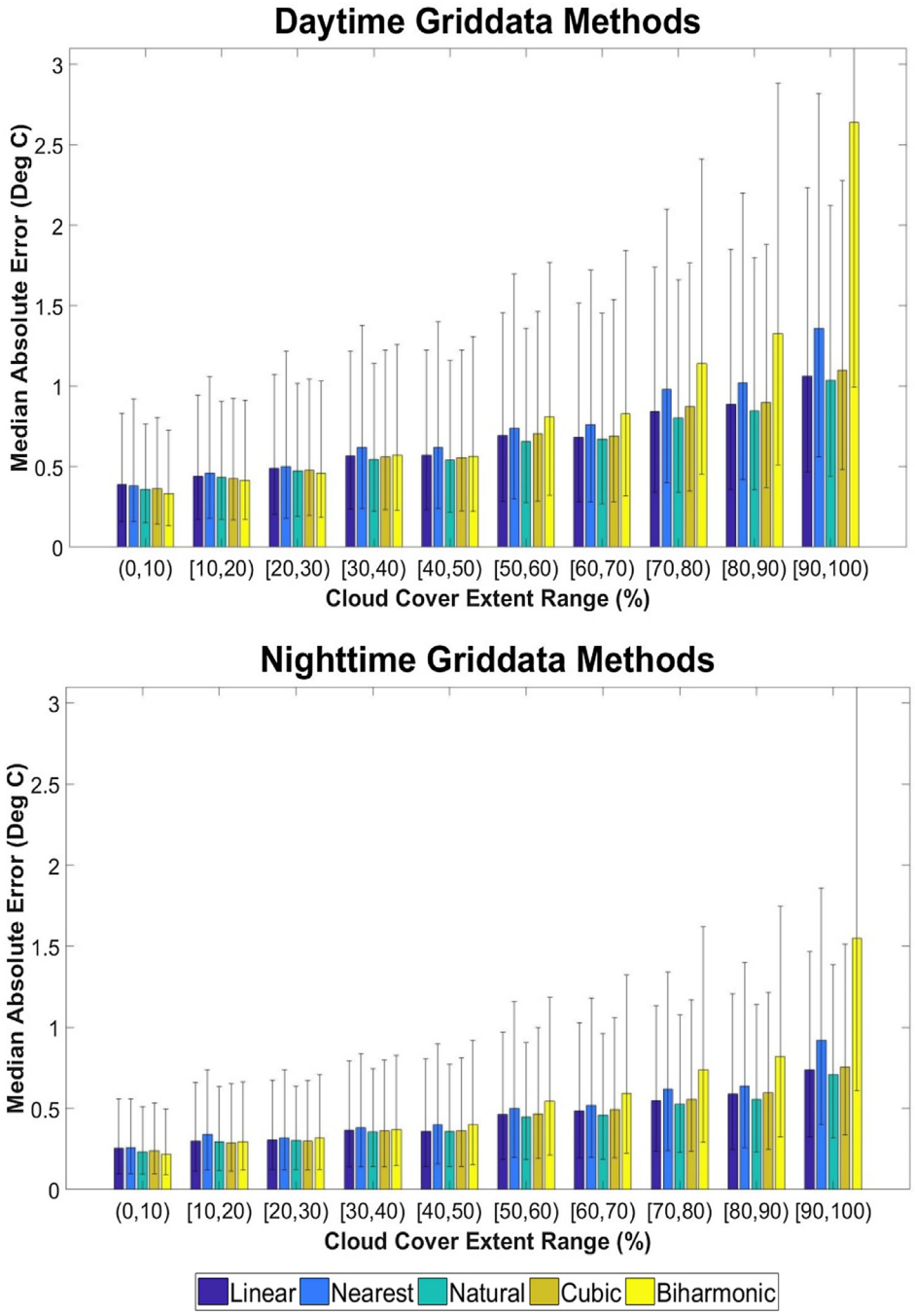

Fig. 8. MAEs and 75th/25th percentiles by percent cloud cover category across all seasons for Matlab *Griddata* methods applied to daytime and nighttime LST. Most bins contain 6800 samples (20 tests at 85 sites for 4 seasons); a small portion of tests (< 2.5%), especially for [90,100%), could not be completed for some methods. Note: 75th percentiles of 7.13 and 3.57 not shown for last category of daytime and nighttime Biharmonic, respectively. Created using function by Callaghan (2014).

Although Spline was the best predictor for the majority of sites at low cloud cover (< 30%), there was a small portion of sites for which other methods were the best. However, these anomalies appeared to be caused by unexplained variability, as opposed to outlying average slopes. The sites differed across seasons, categories, and times of day, and their average slopes were generally not above the 75th pectineal. While Slope had a large, positive standardized coefficient in the Spline and Adaptive Window models, the adjusted R^2s were low, indicating a small portion of variation in MAEs was explained. There does not seem to be a threshold for Slope that at which point, other methods become more predictive than Spline at low cloud cover.

Temp had the largest influence on both daytime and nighttime MAEs for Linear Temporal and HANTS, suggesting temporal methods perform better in warmer climates. We are unable to explain this finding. Given that fewer values neighboring in time decreases the predictive capability of temporal methods, one would expect Percip to have a greater influence. However, this was only significant in the nighttime HANTs models with relatively low coefficient. Similar to Slope, the few sites where temporal methods performed best at high cloud cover was the result of unexplained variation, as opposed unusually high Temp values.

Interestingly, Temp had the largest influence on daytime and nighttime MAEs for Weiss and nighttime Gradient. Slope also had the largest influence daytime Gradient MAEs and was significant in the nighttime Weiss model. Although the standardized coefficients were comparatively smaller, spatiotemporal methods tend to perform worse

in areas with steeper slopes and better in warmer climates, potentially due their utilization of both the spatial and temporal domains.

The magnitude, sign, and significance of land cover coefficients varied by model and did not have the greatest influence on any method's MAEs. The standardized coefficient for PerFor was significant and negative for the daytime and nighttime Spline models, indicating that this method may perform better in areas with greater forest cover. Researchers have found that dense forests stabilize local thermal environments, acting as a thermal buffer (Zhao et al., 2017; Lin et al., 2017). It is possible that this smaller variation in LST increases the accuracy of fit surfaces. While LST can vary across land cover categories, with the exception of forest with Spline, we did not find consistent evidence to indicate certain land cover can influence interpolation.

3.3. Recommendations for implementation

Spline is the easiest method to implement, since spatial interpolation packages are available through numerous platforms, including ArcGIS, SAGA GIS, Matlab, Python, and R; Weiss is more challenging to implement. Although no external data is required, users must build an extensive LST image stack, execute iterative searches for valid pixels in both temporal and spatial domains, and perform multi-directional window averaging if the threshold for valid pixels is not initially met.

Our results indicate that it would be most effective to apply Spline for images with low cloud cover (< 30%) and Weiss for images with greater cover or extensive gaps. Although there were some instances when Adaptive Window and Gradient outperformed Weiss under these circumstances, improvements were typically small (< 0.1 °C). Based on the data used for this analysis, the vast majority of MODIS 8-day LST composites requiring interpolation contain low cloud cover (87% and 89% for daytime and nighttime images, respectively). In fact, most (75% and 77% for daytime and nighttime images, respectively) contain < 10% cloud cover, for which there was substantial separation between the predictive capability of Spline and other methods. Considering the distribution of cloud contamination and difficulty of implementing Weiss, using Spline under all conditions for simplicity would be sufficient. While it is rare (< 0.5%), Linear Temporal could be employed for images with 100% cloud cover. We caution the use of Spline across areas larger than the ones we assessed (approximately 101 by 101 km). If a selected site is larger, it may be necessary to fit surfaces to sub-sections.

We employed the Biharmonic Spline option available with the *Griddata* function in Matlab. However, there are a number of other interpolation options including Linear, Nearest Neighbor, Natural Neighbor, and Cubic Spline. To further investigate the performance of these methods, a similar analysis was performed, only MAEs were computed for each category across all seasons. Biharmonic Spline did not consistently produce the lowest MAE for daytime or nighttime images. In fact, it produced a substantially greater MAE for the last category (Fig. 8). Thus, it is not necessary to employ a particular Spline option or spatial interpolation package, as they appear to be equally effective.

Our analysis utilized images from the MODIS sensor onboard the Terra satellite. Images are also available from the MODIS sensor onboard the Aqua satellite. Their specifications only differ by the overpass time. Terra crosses the equator each day at approximately 10:30 AM and 10:30 PM in local solar time; Aqua crosses at 1:30 AM and 1:30 PM (Reese, 2016). Although MAE values differed slightly between daytime and nighttime images, the performance of the methods did not substantially differ with respect to each other. As there were no major discrepancies, we would expect to derive the same findings with images from the Aqua sensor.

4. Conclusions

This study compared the performance of six methods previously employed to interpolate invalid pixels in 8-day MODIS LST images across various cloud cover extents and seasons. The impact of topographic, land cover, and climatic factors was also assessed. Prior to this work, there had been no empirical comparison of interpolation methods; assessment had been limited to single study area and method. Authors that utilized cloud cover simulation for validation randomly set pixels to invalid and did not consider natural cloud formations or implement a wide range of conditions. In addition, there had been no consideration of factors that may influence prediction. To the best our knowledge, this analytical framework represents the most comprehensive and rigorous assessment to date.

There is strong evidence that the predictive capability of spatial and spatiotemporal methods is superior to temporal methods, even at very high cloud cover. This was the case for both daytime and nighttime LST and across all seasons. Based on the regression analysis, spatial methods appear to be most influenced by topography, such that areas with steeper slopes have higher MAEs. Temporal methods are most influenced by mean annual temperature, with warmer areas having lower MAEs. Due to their consideration of both domains, these factors also influence spatiotemporal methods, but to a lesser extent. With the exception of forest for Spline, land cover did not influence prediction. Although several factors were significant, the assed covariates explained a relatively low portion of variation in MAE values and did not cause a departure from our major findings at sites with extreme values. Based on the distribution of cloud contamination, ease of Spline's implementation, and its improved predicative capability over other methods under low cloud cover (< 30%), we conclude that the use of Spline under all circumstances is sufficient.

While it would be challenging to perform a comprehensive assessment of daily interpolation methods, given the wide range and complexity of proposed methods, a similar framework could be employed to compare some of the more commonly utilized approaches. Although spatial methods were found to work best for 8-day composites, the temporal domain may prove to be more useful at a smaller time step. This analysis could also be expanded to additional sensors that capture thermal infrared radiation, such as AVHRR and AATSR, or study areas beyond the CONUS. Findings from daily images, alternative sensors, and locations beyond the CONUS would provide valuable information to future researchers.

Acknowledgments

This study was supported by NASA's Land Cover Land Use Change Program (grant #: NNX15AD42G) and a Graduate Assistantship awarded through Environmental Resources Engineering Department at the SUNY College of Environmental Science and Forestry.

Appendix A. Supplementary material

Supplementary data associated with this article can be found, in the online version, at https://doi.org/10.1016/j.isprsjprs.2018.06.003.

References

Abouali, M., 2012. MATLAB implementation of Harmonic Analysis of Time Series (HANTS). Matlab File Exchange. <http://www.mathworks.com/matlabcentral/fileexchange/38841-matlab-implementation-of-harmonic-analysis-of-time-series–hants> (accessed on March 20th, 2015).

Akhoondzadeh, M., Saradjian, M.R., 2008. Comparison of land surface temperature mapping using MODIS and ASTER images in semi-arid area. Int. Arch. Photogramm. Remote Sens. Spatial Inform. Sci. 37 (B8), 873–876.

Akther, M.S., Hassan, Q.K., 2011. Remote sensing based estimates of surface wetness conditions and growing degree days over northern Alberta, Canada. Boreal Environ. Res. 16 (1), 407–416.

Alfieri, S.M., De Lorenzi, F., Menenti, M., 2013. Mapping air temperature using time

series analysis of LST: the SINTESI approach. Nonlinear Process. Geophys. 20 (4), 513–527. http://dx.doi.org/10.5194/npg-20-513-2013.
Al-Matari, E.M., Al-Swidi, A.K., Fadzil, H.B., 2014. The moderating effect of broad diversity on the relationship between executive committee characteristics and firm performance in Oman: empirical study. Asian Soc. Sci. 10 (12), 6–20. http://dx.doi.org/10.5539/ass.v10n12p.
Alkorta, I., Barrios, L., Rozas, I., Elguero, J., 2000. Comparison of models to correlate electron density at the bond critical point and bond distance. J. Mol. Struct.: OCHEM 496, 131–137. http://dx.doi.org/10.1016/S0166-1280(99)00177-3.
Bakon, K.A., Hassan, Z., 2013. Perceived value of Smartphone and its impact on deviant behavior: an investigation on higher education students in Malaysia. Int. J. Informat. Syst. Eng. 1 (1), 1–17 ISSN: 2289-2265.
Bikfalvi, A., 2012. Advanced Box Plot for Matlab. <http://alex.bikfalvi.com/research/advanced_matlab_boxplot/> (accessed on April 12th, 2018).
Cai, X., Wang, D., 2006. Spatial autocorrelation of topographic index in catchments. J. Hydrol. 328 (3–4), 581–591. http://dx.doi.org/10.1016/j.jhydrol.2006.01.009.
Callaghan, M., 2014. Barwitherr (errors, varargin). Matlab File Exchange. <https://www.mathworks.com/matlabcentral/fileexchange/30639-barwitherr-errors-varargin-?requestedDomain=www.mathworks.com> (accessed on July 20th, 2017.
Carroll, M.L., Townshend, J.R., DiMiceli, C.M., Noojipady, P., Sohlberg, R.A., 2009. A new global raster water mask at 250 m resolution. Int. J. Digital Earth 2 (4), 291–308. http://dx.doi.org/10.1080/17538940902951401.
Clinton, N., Gong, P., 2013. MODIS detected surface urban heat islands and sinks: global locations and controls. Remote Sens. Environ. 134, 294–304. http://dx.doi.org/10.1016/j.rse.2013.03.008.
Crosson, W.L., Al-Hamdan, M.Z., Hemmings, S.N.J., Wade, G.M., 2012. A daily merged MODIS Aqua-Terra land surface temperature data set for the conterminous United States. Remote Sens. Environ. 119, 315–324. http://dx.doi.org/10.1016/j.rse.2011.12.019.
Fan, X.-M., Liu, H.-G., Liu, G.-H., Li, S.-B., 2014. Reconstruction of MODIS land-surface temperature in a flat terrain and fragmented landscape. Int. J. Remote Sens. 35 (23), 7857–7877. http://dx.doi.org/10.1080/01431161.2014.978036.
Golding, N., Burstein, R., Longbottom, J., Browne, A.J., Fullman, N., Osgood-Zimmerman, A., Hay, S.I., et al., 2017. Mapping under-5 and neonatal mortality in Africa, 2000-15: a baseline analysis for the sustainable development goals. Lancet 390 (1), 2171–2182.
Guo, Z., Wang, S.D., Cheng, M.M., Shu, Y., 2012. Assess the effect of different degrees of urbanization on land surface temperature using remote sensing images. Procedia Environ. Sci. 13, 935–942. http://dx.doi.org/10.1016/j.proenv.2012.01.087.
Hassan, Q.K., Bourque, C.P.-A., Meng, F., Richards, R., 2007a. Spatial mapping of growing degree days: an application of MODIS-based surface temperatures and enhanced vegetation index. J. Appl. Remote Sens. 1 (1), 013511. http://dx.doi.org/10.1117/1.2740040.
Hassan, Q.K., Bourque, C.P.-A., Meng, F., Cox, R.M., 2007b. A wetness index using terrain-corrected surface temperature and normalized difference vegetation index derived from standard MODIS products: an evaluation of its use in a Humid Forest-Dominated Region of Eastern Canada. Sensors 7 (1), 2028–2048.
Hengl, T., Heuvelink, G.B.M., Perčec Tadić, M., Pebesma, E.J., 2012. Spatio-temporal prediction of daily temperatures using time-series of MODIS LST images. Theor. Appl. Climatol. 107 (1–2), 265–277. http://dx.doi.org/10.1007/s00704-011-0464-2.
Huang, S., Jin, S., Dahal, D., Chen, X., Young, C., Liu, H., Liu, S., 2013. Reconstructing satellite images to quantify spatially explicit land surface change caused by fires and succession: a demonstration in the Yukon River Basin of interior Alaska. ISPRS J. Photogramm. Remote Sens. 79, 94–105. http://dx.doi.org/10.1016/j.isprsjprs.2013.02.010.
Jarvis, A., Reuter, H.I., Nelson, A., Guevara, E., 2008. Hole-filled SRTM for the globe Version 4. Available from the CGIAR-CSI SRTM 90m database. Extracted on March 1st, 2017. <https://drive.google.com/drive/folders/0B_J08t5spvd8VWJPbTB3anNHamc>.
Khandelwal, S., Goyal, R., Kaul, N., Mathew, A., 2017. Assessment of land surface temperature variation due to change in elevation of area surrounding Jaipur, India. Egypt. J. Remote Sens. Space Sci. http://dx.doi.org/10.1016/j.ejrs.2017.01.005.
Kilibarda, M., Hengl, T., Heuvelink, G.B.M., Gräler, B., Pebesma, E., Perčec Tadić, M., Bajat, B., 2014. Spatio-temporal interpolation of daily temperatures for global land areas at 1 km resolution. J. Geophys. Res.: Atmos. 119 (5), 2294–2313. http://dx.doi.org/10.1002/2013JD020803.
Klingseisen, B.J., 2010. Spatio-temporal Modeling of Bluetongue Virus Distribution in Northern Australia Based on Remotely Sensed Bioclimatic Variables (PhD Dissertation). Curtin University of Technology, Department of Spatial Sciences.
Kraemer, M.U.G., Perkins, T.A., Cummings, D.A.T., Zakar, R., Hay, S.I., Smith, D.L., Reiner, R.C., 2015. Big city, small world: density, contact rates, and transmission of dengue across Pakistan. J. Roy. Soc. Interface 12 (111), 20150468. http://dx.doi.org/10.1098/rsif.2015.0468.
Land Process Distributed Active Archive Center (LP DAAC), 2014. NASA EOSDIS. Daac2Disk Tool. Extracted on November 5th, 2017. <https://lpdaac.usgs.gov/tools/data_access/daac2disk_web>.
Li, Z., Zhao, L., Fu, Z., 2012. Estimating net radiation flux in the Tibetan Plateau by assimilating MODIS LST products with an ensemble Kalman filter and particle filter. Int. J. Appl. Earth Obs. Geoinf. 19, 1–11. http://dx.doi.org/10.1016/j.jag.2012.04.003.
Lin, H., Chen, Y., Song, Q., Fu, P., Cleverly, J., Magliulo, V., Fan, Z., et al., 2017. Quantifying deforestation and forest degradation with thermal response. Sci. Total Environ. 607–608, 1286–1292. http://dx.doi.org/10.1016/j.scitotenv.2017.07.062.
Linghong, K., Chunqiao, S., Xiali, D., 2012. Reconstructing complete MODIS LST based on temperature gradients in the northeastern Qunghia-Tibet Plateau. In: Proceedings from the 2012 IEEE Geoscience and Remote Sensing Symposium.
Liu, R., Shang, R., Liu, Y., Lu, X., 2017. Global evaluation of gap-filling approaches for seasonal NDVI with considering vegetation growth trajectory, protection of key point, noise resistance and curve stability. Remote Sens. Environ. 189, 164–179. http://dx.doi.org/10.1016/j.rse.2016.11.023.
Longbottom, J., Browne, A.J., Pigott, D.M., Sinka, M.E., Golding, N., Hay, S.I., Shearer, F.M., 2017. Mapping the spatial distribution of the Japanese encephalitis vector, *Culex tritaeniorhynchus* Giles, 1901 (Diptera: Culicidae) within areas of Japanese encephalitis risk. Parasites Vectors 10 (1). http://dx.doi.org/10.1186/s13071-017-2086-8.
Ma, H., Liang, S., Xiao, Z., Shi, H., 2017. Simultaneous inversion of multiple land surface parameters from MODIS optical–thermal observations. ISPRS J. Photogramm. Remote Sens. 128, 240–254. http://dx.doi.org/10.1016/j.isprsjprs.2017.04.007.
Maffei, C., Alfieri, S., Menenti, M., 2012. Characterizing fire hazard from temporal sequences of thermal infrared MODIS measurements. In: 1st EARSeL Workshop on Temporal Analysis of Satellite Images.
Mathew, A., Khandelwal, S., Kaul, N., 2017. Investigating spatial and seasonal variations of urban heat island effect over Jaipur city and its relationship with vegetation, urbanization and elevation parameters. Sustain. Cities Soc. 35, 157–177. http://dx.doi.org/10.1016/j.scs.2017.07.013.
Messina, J.P., Pigott, D.M., Golding, N., Duda, K.A., Brownstein, J.S., Weiss, D.J., Hay, S.I., 2015. The global distribution of Crimean-Congo hemorrhagic fever. Trans. Roy. Soc. Tropical Med. Hygiene 109 (8), 503–513. http://dx.doi.org/10.1093/trstmh/trv050.
Metz, M., Rocchini, D., Neteler, M., 2014. Surface temperatures at the continental scale: tracking changes with remote sensing at unprecedented detail. Remote Sens. 6 (5), 3822–3840. http://dx.doi.org/10.3390/rs6053822.
Michishita, R., Jin, Z., Chen, J., Xu, B., 2014. Empirical comparison of noise reduction techniques for NDVI time-series based on a new measure. ISPRS J. Photogramm. Remote Sens. 91, 17–28. http://dx.doi.org/10.1016/j.isprsjprs.2014.01.003.
Mylne, A.Q.N., Pigott, D.M., Longbottom, J., Shearer, F., Duda, K.A., Messina, J.P., Hay, S.I., et al., 2015. Mapping the zoonotic niche of Lassa fever in Africa. Trans. Roy. Soc. Tropical Med. Hygiene 109 (8), 483–492. http://dx.doi.org/10.1093/trstmh/trv047.
Neteler, M., 2010. Estimating daily land surface temperatures in mountainous environments by reconstructed MODIS LST data. Remote Sens. 2 (12), 333–351. http://dx.doi.org/10.3390/rs1020333.
Nsoesie, E.O., Kraemer, M.U., Golding, N., Pigott, D.M., Brady, O.J., Moyes, C.L., Brownstein, J.S., 2016. Global distribution and environmental suitability for chikungunya virus, 1952 to 2015. Eurosurveillance 21 (20). http://dx.doi.org/10.2807/1560-7917.ES.2016.21.20.30234.
Omernik, J.M., Griffith, G.E., 2014. Ecoregions of the conterminous United States: evolution of a hierarchical spatial framework. Environ. Manage. 54 (6), 1249–1266. http://dx.doi.org/10.1007/s00267-014-0364-1.
Pigott, D.M., Golding, N., Mylne, A., Huang, Z., Weiss, D.J., Brady, O.J., Hay, S.I., 2015. Mapping the zoonotic niche of Marburg virus disease in Africa. Trans. Roy. Soc. Tropical Med. Hygiene 109 (6), 366–378. http://dx.doi.org/10.1093/trstmh/trv024.
Poggio, L., Gimona, A., Brown, I., 2012. Spatio-temporal MODIS EVI gap filling under cloud cover: an example in Scotland. ISPRS J. Photogramm. Remote Sens. 72, 56–72. http://dx.doi.org/10.1016/j.isprsjprs.2012.06.003.
PRISM Climate Group, 2004. Oregon State University. Extracted on March 2nd, 2017 from <http://prism.oregonstate.edu>.
Qiao, Z., Tian, G., Xiao, L., 2013. Diurnal and seasonal impacts of urbanization on the urban thermal environment: a case study of Beijing using MODIS data. ISPRS J. Photogramm. Remote Sens. 85, 93–101. http://dx.doi.org/10.1016/j.isprsjprs.2013.08.010.
Qingbai, W., Yongzhi, L., 2004. Ground temperature monitoring and its recent change in Qinghai-Tibet Plateau. Cold Reg. Sci. Technol. 38 (2–3), 85–92. http://dx.doi.org/10.1016/S0165-232X(03)00064-8.
Rahaman, K.R., Hassan, Q.K., 2017. Quantification of local warming trend: a remote sensing-based approach. PLOSE ONE 10 (1), 3–18.
Rahman, K.M., 2011. Remote Sensing-based Determination of Deciduous and Understory Phenology Over Boreal Forests (Master's Thesis). SCHLUCHI, Department of Geomatics Engineering.
Reese, M., 2016. "Near Real-Time Data Frequently Asked Questions." EOSDIS Support Knowledge base. <https://wiki.earthdata.nasa.gov/display/ESKB/Near+Real-Time+Data+Frequently+Asked+Questions> (accessed on August 8th).
Ren, H., Yan, G., Chen, L., Li, Z., 2011. Angular effect of MODIS emissivity products and its application to the split-window algorithm. ISPRS J. Photogramm. Remote Sens. 66 (4), 498–507. http://dx.doi.org/10.1016/j.isprsjprs.2011.02.008.
Ren, J., Chen, Z., Zhou, Q., Tang, H., 2008. Regional yield estimation for winter wheat with MODIS-NDVI data in Shandong, China. Int. J. Appl. Earth Obs. Geoinf. 10 (4), 403–413. http://dx.doi.org/10.1016/j.jag.2007.11.003.
Roerink, G.J., Menenti, M., Verhoef, W., 2000. Reconstructing cloudfree NDVI composites using Fourier analysis of time series. Int. J. Remote Sens. 21 (9), 1911–1917. http://dx.doi.org/10.1080/014311600209814.
Liang, Shunlin, 2001. An optimization algorithm for separating land surface temperature and emissivity from multispectral thermal infrared imagery. IEEE Trans. Geosci. Remote Sens. 39 (2), 264–274. http://dx.doi.org/10.1109/36.905234.
Shwetha, H.R., Kumar, D.N., 2016. Prediction of high spatio-temporal resolution land surface temperature under cloudy conditions using microwave vegetation index and ANN. ISPRS J. Photogramm. Remote Sens. 117, 40–55. http://dx.doi.org/10.1016/j.isprsjprs.2016.03.011.
Stroppiana, D., Antoninetti, M., Brivio, P.A., 2014. Seasonality of MODIS LST over Southern Italy and correlation with land cover, topography and solar radiation. Eur. J. Remote Sens. 47 (1), 133–152. http://dx.doi.org/10.5721/EuJRS20144709.
Tang, C.-S., Shi, B., Gao, L., Daniels, J.L., Jiang, H.-T., Liu, C., 2011. Urbanization effect on soil temperature in Nanjing, China. Energy Build. 43 (11), 3090–3098. http://dx.

doi.org/10.1016/j.enbuild.2011.08.003.
Tomlinson, C.J., Chapman, L., Thornes, J.E., Baker, C., 2011. Remote sensing land surface temperature for meteorology and climatology: a review: remote sensing land surface temperature. Meteorol. Appl. 18 (3), 296–306. http://dx.doi.org/10.1002/met.287.
United States Department of Commerce (US DOC), 2002. Climate Reference Network: Site Information Handbook. NOAA-CRN/OSD-2002-0002R0UD0. <https://www1.ncdc.noaa.gov/pub/data/uscrn/documentation/program/X030FullDocumentD0.pdf>.
United States Environmental Protection Agency (US EPA), 2013. US Level III Ecoregions shapefile without states boundaries. <https://www.epa.gov/eco-research/level-iii-and-iv-ecoregions-continental-united-states> (accessed on April 21st, 2017).
United States Geological Survey (USGS), 2017. National Land Cover Database 2011, Product Legend. <https://www.mrlc.gov/nlcd11_leg.php> (accessed on: March 2nd, 2017).
Van De Kerchove, R., Lhermitte, S., Veraverbeke, S., Goossens, R., 2013. Spatio-temporal variability in remotely sensed land surface temperature, and its relationship with physiographic variables in the Russian Altay Mountains. Int. J. Appl. Earth Obs. Geoinf. 20, 4–19. http://dx.doi.org/10.1016/j.jag.2011.09.007.
Van Nguyen, O., Kawamura, K., Trong, D.P., Gong, Z., Suwandana, E., 2015. Temporal change and its spatial variety on land surface temperature and land use changes in the Red River Delta, Vietnam, using MODIS time-series imagery. Environ. Monit. Assess. 187 (7). http://dx.doi.org/10.1007/s10661-015-4691-3.
Venkathaialam, V., Abdulwahab, A.S., 2017. The impact of digitization of retail banks in Malaysia on customer experience. Int. J. Acc. Bus. Manage. 5 (2), 197–213 24924/ijabm/2017.011/v5.iss2/197.213.
Wan, Z., 2008. New refinements and validation of the MODIS land-surface temperature/emissivity products. Remote Sens. Environ. 112 (1), 59–74. http://dx.doi.org/10.1016/j.rse.2006.06.026.
Weiss, D.J., Mappin, B., Dalrymple, U., Bhatt, S., Cameron, E., Hay, S.I., Gething, P.W., 2015. Re-examining environmental correlates of *Plasmodium falciparum* malaria endemicity: a data-intensive variable selection approach. Malar. J. 14 (1), 68. http://dx.doi.org/10.1186/s12936-015-0574-x.
Weiss, D.J., Atkinson, P.M., Bhatt, S., Mappin, B., Hay, S.I., Gething, P.W., 2014. An effective approach for gap-filling continental scale remotely sensed time-series. ISPRS J. Photogramm. Remote Sens. 98, 106–118. http://dx.doi.org/10.1016/j.isprsjprs.2014.10.001.
Wu, C.-D., Lung, S.-C.C., Jan, J.-F., 2013. Development of a 3-D urbanization index using digital terrain models for surface urban heat island effects. ISPRS J. Photogramm. Remote Sens. 81, 1–11. http://dx.doi.org/10.1016/j.isprsjprs.2013.03.009.
Xu, Y., Shen, Y., 2013. Reconstruction of the land surface temperature time series using harmonic analysis. Comput. Geosci. 61, 126–132. http://dx.doi.org/10.1016/j.cageo.2013.08.009.
Xu, Y., Shen, Y., Wu, Z., 2013. Spatial and temporal variations of land surface temperature over the tibetan plateau based on harmonic analysis. Mt. Res. Dev. 33 (1), 85–94. http://dx.doi.org/10.1659/MRD-JOURNAL-D-12-00090.1.
Yu, W., Ma, M., Wang, X., Tan, J., 2014. Estimating the land-surface temperature of pixels covered by clouds in MODIS products. J. Appl. Remote Sens. 8 (1), 083525. http://dx.doi.org/10.1117/1.JRS.8.083525.
Yu, W., Nan, Z., Wang, Z., Chen, H., Wu, T., Zhao, L., 2015. An effective interpolation method for MODIS land surface temperature on the Qinghai-Tibet plateau. IEEE J. Sel. Top. Appl. Earth Obs. Remote Sens. 8 (9), 4539–4550. http://dx.doi.org/10.1109/JSTARS.2015.2464094.
Zakerian, S.A., Subramaniam, I.D., 2009. The relationship between physiological work factors, work stress and computer-related musculoskeletal discomforts among computer users in Malaysia. Int. J. Occupat. Safety Ergon. 15 (4), 425–434. http://dx.doi.org/10.1080/10803548.2009.11076822.
Zeng, Chao, Shen, Huanfeng, Zhong, Mingliang, Zhang, Liangpei, Penghai, Wu., 2015. Reconstructing MODIS LST based on multitemporal classification and robust regression. IEEE Geosci. Remote Sens. Lett. 12 (3), 512–516. http://dx.doi.org/10.1109/LGRS.2014.2348651.
Zeng, L., Wardlow, B.D., Wang, R., Shan, J., Tadesse, T., Hayes, M.J., Li, D., 2016. A hybrid approach for detecting corn and soybean phenology with time-series MODIS data. Remote Sens. Environ. 181, 237–250. http://dx.doi.org/10.1016/j.rse.2016.03.039.
Zhang, G., Xiao, X., Dong, J., Kou, W., Jin, C., Qin, Y., Biradar, C., 2015. Mapping paddy rice planting areas through time series analysis of MODIS land surface temperature and vegetation index data. ISPRS J. Photogramm. Remote Sens. 106, 157–171. http://dx.doi.org/10.1016/j.isprsjprs.2015.05.011.
Zhang, L., Huang, J., Guo, R., Li, X., Sun, W., Wang, X., 2013. Spatio-temporal reconstruction of air temperature maps and their application to estimate rice growing season heat accumulation using multi-temporal MODIS data. J. Zhejiang Univ. Sci. B 14 (2), 144–161. http://dx.doi.org/10.1631/jzus.B1200169.
Zhao, Z.-Q., He, B.-J., Li, L.-G., Wang, H.-B., Darko, A., 2017. Profile and concentric zonal analysis of relationships between land use/land cover and land surface temperature: case study of Shenyang, China. Energy Build. 155, 282–295. http://dx.doi.org/10.1016/j.enbuild.2017.09.046.
Zhou, J., Jia, L., Menenti, M., Gorte, B., 2016. On the performance of remote sensing time series reconstruction methods – a spatial comparison. Remote Sens. Environ. 187, 367–384. http://dx.doi.org/10.1016/j.rse.2016.10.025.